Sound & Vibration 2025, 59(1), 1805.
https://doi.org/10.59400/sv1805

Article

Acoustic multi-objective optimization of porous media properties of a diesel particulate filter

Sinem Ozturk, Haluk Erol*

Mechanical Engineering Faculty, Istanbul Technical University, Istanbul 34439, Turkey
*** Corresponding author:** Haluk Erol, erolha@itu.edu.tr

CITATION

Ozturk S, Erol H. Acoustic multi-objective optimization of porous media properties of a diesel particulate filter. Sound & Vibration. 2025; 59(1): 1805. https://doi.org/10.59400/sv1805

ARTICLE INFO

Received: 29 September 2024
Accepted: 25 October 2024
Available online: 21 November 2024

Abstract: Studies on emission control systems have proliferated because of increasing environmental regulations in recent decades. One of the most important emission control systems in vehicles is the Diesel Particulate Filter (DPF). DPFs are important for not only the harmful emission of soot particles but also acoustic emissions. In this study, the acoustic behavior of DPFs was investigated. The study presents an acoustic multi-objective optimization of the porous media properties of a DPF. The multi-objective optimization was performed using the Non-Dominated Sorting Genetic Algorithm (NSGA-II) to obtain an optimum DPF design. In this study, we aimed to maximize the acoustic transmission losses (TL) of the DPF and minimize the pressure drop according to the porous media properties. The DPF wall permeability, channel width, channel wall thickness and channel number were chosen from the porous media properties as design variables for the optimization problem. Test studies have been conducted to validate the mathematical model utilized in optimization. Following these investigations, it has been concluded that the mathematical model, verified through experimental research, is now considered a viable model for resolving the optimization problem. As a result, an optimum DPF design that provides both objective functions was proposed.

Keywords: Diesel Particulate Filter (DPF); Acoustic Transmission Loss (TL); multi-objective optimization; porous media; Non-Dominated Sorting Genetic Algorithm (NSGA-II)

1. Introduction

Diesel Particulate Filters play an important role in the automobile industry due to developments in diesel engines. They are used to reduce the harmful emission of soot particles and affect acoustic emissions. In recent decades, DPFs have been a subject of interest for acoustics researchers. There have been many studies on the acoustics, flow properties and optimization of DPFs. Konstandopoulous et al. [1] built a mathematical model to investigate the pressure drop and filtration characteristics of wall-flow DPFs. They modeled the flow through a porous medium by Darcy's Law. The first attempt to conduct acoustic modeling and testing of the DPF in the literature was made by Allam and Abom [2]. They built two models, a lumped model valid for low frequencies and a detailed model valid for the entire plane wave range, to describe the acoustic behavior of DPFs. Dokumaci [3] studied the propagation of plane sound waves in pipes with porous walls. In that study, general numerical and approximate analytical solutions were proposed. Wenzhi and Liming [4] studied the acoustic performance of the DPF and developed a FEM model to analyze its sound propagation characteristics. This approach is a combination of finite element analysis and viscosity correction. Fayyad et al. [5] presented a 2D model to calculate the wave propagation constant and acoustic impedance of the DPF unit. The obtained results are in good

agreement with those presented by other investigators. Liu and Miller [6] performed an analytical and numerical study of wall-flow filters with equilateral triangular channels. The flow fields of these filters were modeled analytically using a one-dimensional approach and simulated numerically using a three-dimensional approach. The flow distributions and pressure drops were presented and discussed in their study. Katari et al. [7] studied the effect of filter parameters, such as the aspect ratio. An extension of this study includes the effect of the inlet and outlet cones on the contraction and expansion of flow at the inlet and exit of the filter channels. The study covers both cordierite and silicon carbide (SiC) diesel exhaust particulate filters.

Recent advancements in Diesel Particulate Filters (DPFs) have focused on improving regeneration mechanisms, filtration efficiency, and emission control. Zhang et al. (2023) reviewed modern DPF technologies and highlighted the role of advanced regeneration strategies in reducing particulate matter (PM) emissions from diesel engines, emphasizing structural innovations and material developments that enhance filter durability and performance [8]. In a related study, Tan et al. (2020) proposed an extended filtration model based on the morphology characteristics of diesel particulates, offering a more accurate prediction of filter efficiency by introducing a global filtration correction coefficient [9]. Lisi et al. (2020) critically reviewed the role of soot-catalyst interaction in catalytic DPFs, underlining the challenges in optimizing soot oxidation during passive regeneration to improve overall system performance [10]. Zhang et al. [11] conducted a grey correlation analysis to investigate the influence of structural parameters on DPF trapping performance, finding that filter diameter, length, and cell density significantly impact both pressure drop and filtration efficiency. Finally, Meng et al. [12] explored the emission characteristics of catalytic DPFs during passive regeneration, demonstrating that commercial carbon black can effectively simulate soot behavior in experimental setups, providing insights into improving DPF design for heavy-duty applications.

The porous media properties of the DPF were also investigated in the literature. One such study was by Payri et al. [13], who developed a methodology that uses pressure drop measurements to determine the structural properties of the hole, such as the permeability, porosity and pore size. Fayyad [14] presented a new technology to reduce the emissions and noise of exhaust internal combustion engines using DPF. The relationships between the transmission losses and wall thickness, porosity, permeability and pressure drop were determined in that study. Momani [15] studied the effect of the porous media properties on the sound propagation and transmission losses through such materials and consequently on the noise reduction factor. Sprouse III et al. [16] developed two methods for simultaneously solving the differential conservation equations along with the algebraic ideal gas law in the inlet and outlet channels. They used four permeability models from different disciplines in Darcy's law to determine their applicability in calculating DPF wall velocity profiles. Stratakis et al. [17] presented the results of an experimental analysis of pressure drop as a function of the geometric and operating parameters of cordierite and SiC diesel filters. The results were shown to improve the understanding of the effects of partial regeneration and fuel additive residuals on the filter back pressure and flow and soot loading distribution. Masoudi et al. [18] conducted experiments to modify, customize and validate a model yielding accurate predictions of a ceramic wall-flow DPF

pressure drop. The model accounts for not only the major pressure drop components due to channel plugs, flow contraction and expansion due to the flow entering and exiting the trap but also flow secondary inertial effects near the porous walls.

Some studies optimize the DPF for a few parameters by changing only one parameter value and keeping the others stable. Michelin et al. carried out a comparative optimization for the DPF regeneration [19]. Consequently, a DPF made of SiC has higher physical durability than one made of cordierite. Barataud et al. [20] carried out specific tests and presented a new silicon carbide DPF, which not only increased durability but also reduced cost. Ozturk and Erol [21] carried out a multi-objective optimization of a DPF by an acoustic approach. Jun et al. [22] studied optimizing a DPF structure with a good flow field distribution by considering the exterior restriction conditions such as the chassis space, exhaust pipe diameter and diesel engine displaced volume. Using a FLUENT solver, they determined parameters such as the diameter ratio and dilation angle for an optimum DPF. Fujii et al. [23] proposed a simulator composed of diesel fuel burners for fundamental DPF evaluations. Hicks et al. [24] physically tested DPFs with various substrate materials, catalytic coatings, and soot loadings to gather data that can be applied during the exhaust system development process. They used this information to aid in developing computer models for acoustic and engine performance predictive software. This study proposes an optimum DPF design with the maximum TL and minimum pressure drop using the 1-D model. In the scope of this goal, the porous media properties of a DPF were examined in detail. After specifying the porous media properties, a multi-objective optimization was carried out to determine the optimum parameter values. Maximizing the TL and minimizing the pressure drop were defined as the two objective functions for the optimization problem. This study differs from other DPF optimization studies in that the optimization was performed for more than one parameter simultaneously, while the others changed only one parameter value at a time while keeping the others stable.

2. Theory

The wall-flow monolith DPF is the most common design. It has many small parallel channels running in the axial direction, usually a cylindrical ceramic structure. The walls of the channels are porous, and adjacent channels are plugged at each end to cause gas to flow through these porous walls. The flow pattern is shown in **Figure 1**.

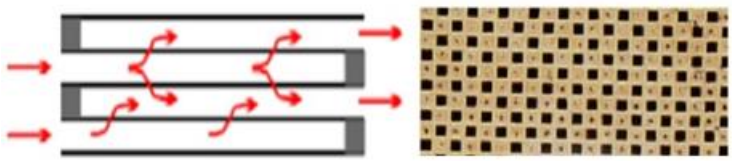

Figure 1. Neighboring channels in the DPF.

Because flow through the porous wall is out of the question, mentioning the porous media properties is necessary. The DPF channel width, wall permeability,

channel number and DPF channel wall thickness are among the porous media properties of the DPF.

There are two suggested models for the flow in porous media; one belongs to Darcy and the other belongs to Brinkman. To describe the flow of fluids through porous media, Darcy's Law for one-dimensional flow in porous media applies,

$$Q = -\left(\frac{\sigma A}{\mu}\right)\left(\frac{\Delta P}{L}\right) \tag{1}$$

where Q is the fluid flow rate through the medium, σ is the permeability, A is the cross-sectional area, μ is the fluid viscosity, ΔP is the pressure gradient, and L is the length. For many applications, the most important physical property of the porous media is wall permeability. Permeability is part of the proportionality constant in Darcy's law, which relates flow rate and viscosity to a pressure gradient applied to the porous media:

$$\sigma = \frac{Q\mu\Delta x}{A\Delta p} \tag{2}$$

where Q is the volumetric flow rate, A is the area, μ is the dynamic viscosity of the fluid, Δp is the applied pressure difference and Δx is the thickness of the bed of the porous medium.

The second model that describes a permeable medium, the Brinkman equation, is expressed as

$$\Delta P = -\frac{\mu}{\sigma}V + \mu_e \nabla^2 V \tag{3}$$

Here V is the fluid velocity, μ is the fluid viscosity, μ_e is the effective fluid viscosity, σ is permeability and ΔP is the pressure drop. The pressure drop is one of the most critical DPF parameters to achieve good fuel economy. The pressure drop in the DPF is affected by DPF parameters such as wall thickness and permeability. The total pressure drop for a loaded filter can be divided into four parts: the pressure drop of the inlet channel, the pressure drop of the outlet channel, the pressure drop across the soot layer, and the pressure drop across the substrate wall [20]. The basic pressure drop equation for a clean filter (w_s) is shown below:

$$\Delta P_{clean} = \frac{\mu}{k_0}\frac{U\alpha}{4L}w + \frac{2\mu F}{3\alpha^2}UL \tag{4}$$

In this equation, μ is the exhaust dynamic viscosity, F is a factor equal to 28.454, L is the length of the filter, k_0 is the clean filter wall permeability, and U is the inlet velocity. The inlet velocity can be written in terms of the filter diameter D_f, the actual exhaust volumetric flow rate Q and the filter cell density ρ as:

$$U = \frac{8Q}{\pi D_f^2 \rho \alpha^2} \tag{5}$$

$$\rho = \frac{1}{\left(\alpha + w\right)^2} \tag{6}$$

where α is the filter cell width and w is the wall thickness. The total volume of the filter is

$$V_{trap} = \frac{\pi D_f^2 L}{4} \tag{7}$$

Thus, the pressure drop for the clean DPF can be written as:

$$\Delta P = \frac{\mu Q}{2V_{trap}}(\alpha + w)^2 \left(\frac{w}{k_0 \alpha} + \frac{8FL^2}{3\alpha^4}\right) \tag{8}$$

To determine the acoustic performance of the DPF, transmission loss is the critical parameter. The transmission loss (*TL*) is generally defined as the difference between the incident power and that transmitted downstream into an anechoic termination. It can be calculated as;

$$TL = 10\ log\ log\ (W_i/W_t) \tag{9}$$

Here, W_i is the incident power and W_t is the transmitted power. For the DPF unit, the *TL* can be calculated as

$$TL = 20\ log\ log\ (0.5|T_{DPF}|) \tag{10}$$

where T_{DPF} is the transfer matrix of the DPF. A DPF unit cell can be divided into five sections: input (IN), a short plug with impermeable walls (I); a filter section having channels with porous walls (II); a short plug with impermeable walls (III) and the output.

Considering these sections shown in **Figure 2**, the transfer matrix for a DPF is

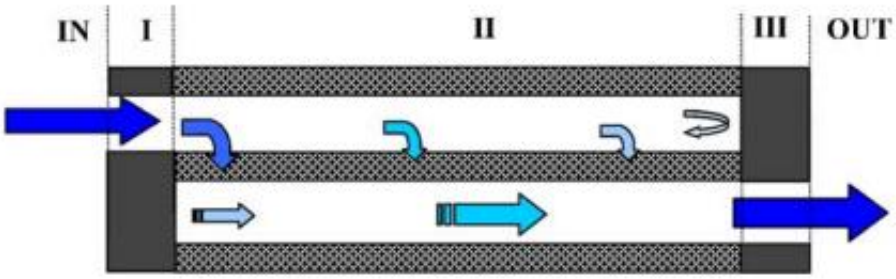

Figure 2. Cross-section of a unit cell in a split DPF.

$$T_{DPF} = T_{IN} T_I T_{II} T_{III} T_{OUT} \tag{11}$$

and by using the continuity and momentum equations, the *TL* for a DPF unit can be calculated as;

$$TL = 10\left\{\left(\frac{1 + M_{in}}{1 + M_{out}}\right)^2 \frac{Z_{in}}{4Z_{out}} |T_{11}^{DPF} + \frac{T_{12}^{DPF}}{Z_{out}} + Z_{in} T_{21}^{DPF} + \frac{Z_{in} T_{22}^{DPF}}{Z_{out}}|^2\right\} \tag{12}$$

In this study, a multi-objective optimization is carried out for the DPF. A general Multi-Objective Optimization Problem is formally defined as minimizing (or maximizing)

$$F(x) = (f_1(x), ..., f_k(x)) \tag{13}$$

subject to

$$g_i(x) \leq 0, i = \{1, \ldots, m\}\ and\ h_j(x) = 0, j = \{1, \ldots., p\} \tag{14}$$

where $f_i(x)$ is an objective function, m is the number of inequality constraints, and p is the number of equality constraints. A Multi-objective Optimization Problem solution minimizes (or maximizes) the components of a vector $x = (x_1, \ldots, x_n)$. These optimal solutions are called Pareto optimal solutions. The Pareto Optimal Solution is not unique; there exists a set of solutions known as the Pareto Optimal Set for a Multi-Objective Optimization.

This study uses the Non-dominated Sorting Genetic Algorithm (NSGA-II) to optimize the DPF. The algorithm starts with a randomly generated population (P_0). Each solution is assigned a fitness (or rank) equal to its non-domination level, and a minimization of the fitness is assumed. First, by using binary tournament selection and recombination and mutation operators, an offspring population of Q_0 is created with a size N (population size). After this step, an elitist strategy is implemented [25].

For a generation (t), a combined population of $R_t = P_t \cup Q_t$ is first formed, with a size of $2N$. Then, R_t is sorted according to non-domination and grouped. The best non-dominated set is called F_1, the second-best is called F_2, and so on. The first set (F_j) of the sum of individuals (beginning from F_1) is determined. F_j is sorted based on the crowding distance and k of the individuals F_j (where $k = \sum_{i=1}^{j-1} |F_i|$) are passed on to generation $t + 1$ [26].

3. Test studies

The test setup in **Figure 3** is detailed, including the arrangement and the equipment utilized. The flow speed during measurements was controlled using a frequency converter attached to an air bellow, allowing precise air velocity control. A pre-silencer was incorporated into the setup to mitigate noise interference from the air bellows. Flow rates were measured using a venturi tube, with the pressure difference across the venturi throat being recorded. These data were subsequently used to calculate mass flow rates using established equations. The microphone placement and the sound source provided consistent acoustic signals, and multiple repetitions of each test were carried out to ensure reproducibility. Additionally, systematic microphone repositioning during repeated measurements minimized phase misalignment between the microphones. Ambient noise isolation was applied to the test environment, and the difference between the noise source and the ambient noise levels was kept above the 20 dB standard. These efforts ensured the measurements reflected the diesel particulate filters' actual transmission loss and pressure drop characteristics under varying conditions.

A Net dB analyzer from the company 01dB and its dBFA Suite software were employed as the Fast Fourier Transform (FFT) converter and the white noise signal generator, respectively. The number of points for the FFT transformation was 1024, with a frequency resolution of 12.5 Hz. Dependent on the frequency range of interest, the bandwidth is 5 kHz. To avoid adverse effects such as signal leakage, "Hanning window" filtering was utilized. Considering the conditions of the environment where measurements were conducted, the measurement duration was averaged to be 4 seconds. G.R.A.S brand Type 46BD pressure-type 1/4 inch microphones were used for collecting time-dependent signals, and these were positioned perpendicularly to

the channel axis with the help of adapters. The measurement setup has been dimensioned according to the principles found in ASTM E 1050–08 and ISO 10534-2 standards. The working range can be specified to determine the lower-frequency f_i and the upper-frequency f_u.

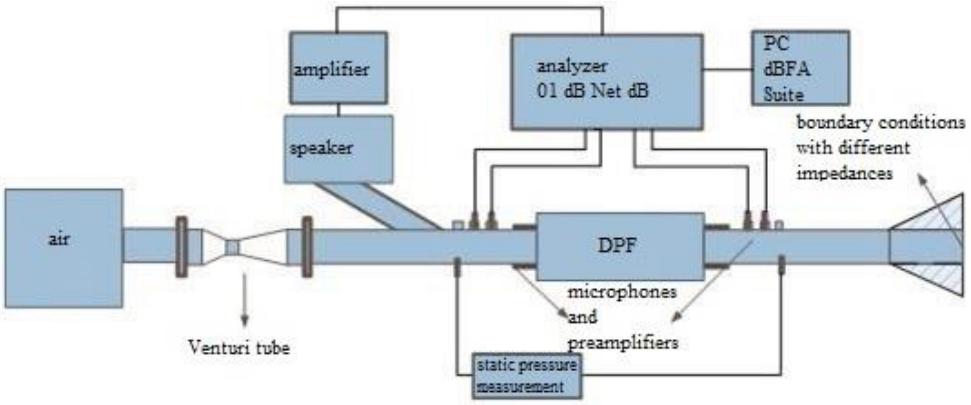

Figure 3. STL test setup.

$$f_i < f < f_u \tag{15}$$

The principle in determining the lower frequency is to establish the microphone diameters (d_{mic}) and the distance between the microphones so that it does not disrupt the theoretical foundation upon which the system is built. Here, λ denotes the wavelength, λ_1 is the highest wavelength, s is the distance between the microphones, and c_0 represents the speed of sound.

$$\begin{matrix} 0.005\lambda_1 < s \quad ISO\ 10534-2 \\ 0.001\lambda_1 < s \quad ASTM\ E\ 1050-08 \end{matrix} \tag{16}$$

$$\lambda = \frac{c_0}{f};\ c_0 = 343{,}2T_{293} \quad T:[K] \tag{17}$$

The principle in determining the upper frequency is to ensure that, in accordance with the one-dimensional plane wave approximation, the sound waves smaller than the diameter are sufficiently large compared to the cross-sectional plane. Movements on the plane at high frequencies result in the equations being invalid. The relevant standards express this criterion as follows.

$$f_u = Kc/d\ K{=}0.586\ (ASTM\ E\ 1050\text{-}08) \tag{18}$$

where d is the diameter of the channel where the microphones are placed, constituting the experimental setup. Similarly, the microphones must be at least a 3d distance from the nearest sound source, and the filter must be at a minimum distance of d. For similar reasons, the gap between microphones is limited by the following expression.

$$s \ll c/2f_u = d/2K \tag{19}$$

Considering the criteria described above, using two different diameters is necessary to evaluate diesel particulate filters across a wide bandwidth. However, since noises at high frequencies can mostly be blocked, the transmission loss in the low-frequency range (between 50~2000 Hz) becomes of interest regarding diesel particulate filter design.

In dimensioning the test system, based on the above discussions, the microphones have been positioned with distances between them set at 30 mm and 60 mm in accordance with other specified values.

The air bellow was used to create air at the desired speed for flow and acoustic measurements. Flow speeds were adjusted by controlling the revolutions per minute with a frequency converter. A pre-silencer was used in the system to prevent the noise created by the air bellows and the noise propagating along the flow from suppressing the noise generated by the speaker. A venturi tube suitable for the system was designed to measure flow speed. The pressure difference at the entrance and the throat section is a function of the geometry of the venturi and the speed. The mass flow rate is calculated using Equation (20), based on the measured pressure difference values. Other characteristics of the venturi tube were determined using standards and manufactured accordingly.

$$q_m = \frac{C}{\sqrt{1-\beta^4}}\,\varepsilon\frac{\pi}{4}{d_b}^2\sqrt{2\Delta P_v \rho_1} \tag{20}$$

In this equation, the terms q_m, C, β, ε, d_b, ΔP_v and ρ_1, respectively, represent the mass flow rate, discharge coefficient, diameter ratio, expansion factor, throat diameter, pressure difference measured in the venturi, and density at the inlet. Using the inlet diameter and density value of the diesel particulate filter, the inlet velocity to the diesel particulate filter can be calculated from the mass flow rate. The discharge coefficient denoted by C accounts for pressure losses in the venturi, while the expansion factor denoted by ε are coefficients related to changes in the properties of air. These values depend on the geometry of the venturi tube and the fluid's properties and are determined based on expressions obtained experimentally through standards.

Tests were conducted for various speeds, and through the least squares method, pressure loss graphs for four diesel particulate filters were obtained for each test (**Figure 4**).

Figure 4. Pressure test setup.

To conceptualize the optimization problem, let us examine how the pressure loss parameter is theoretically calculated. **Figure 5** schematically shows the model of the flow progressing along a DPF's channel and the elements causing pressure loss.

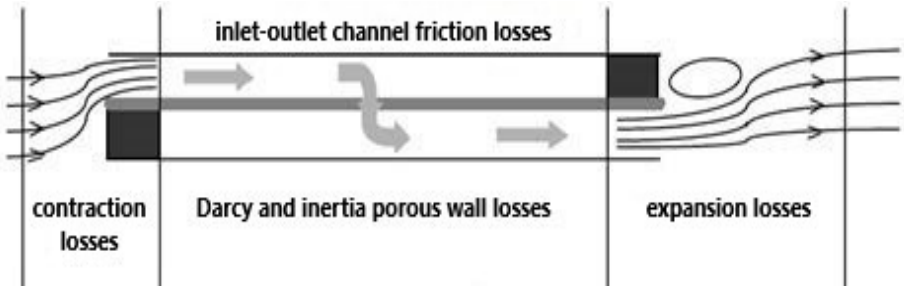

Figure 5. Model of the flow progressing along a DPF's channel and the elements causing pressure loss.

For a clean DPF, the pressure loss can be calculated as the sum of the pressure loss components seen in **Figure 5** [27]. Each component causing pressure loss is dependent on multiple parameters.

The contribution of a porous thin wall to pressure loss can be defined as the sum of the Darcy and Forchheimer terms:

$$\Delta P_{wall} = \frac{\mu}{k} u_w w_s + \beta \rho {u_w}^2 w_s \tag{21}$$

In Equation (21), the parameters used to estimate the pressure loss are the *Darcy permeability k* and the Forchheimer coefficient β. The permeability has the dimension of length squared, and k represents the pore-level length scale, characteristic of the porous medium. The Forchheimer coefficient has the dimension of inverse length and represents the "hole roughness". Both parameters, the Darcy permeability k and the Forchheimer coefficient β, depend on the "hole size" and the permeability of the porous medium.

$$\beta = \frac{cons.}{\varsigma^{1.5}\sqrt{k}} \tag{22}$$

The constant in Equation (22) can be taken as 0.143 or 0.134 for smooth surfaces; for rough surfaces, it can be 0.298. It should be emphasized that the permeability and the Forchheimer coefficient are effective properties of the porous medium and are independent of the size of the measured sample for a homogeneous medium.

Considering the correlation between β and k is valid for granular porous media and fibrous media. Given the known structural properties and operating conditions of DPFs, it can be stated that Forchheimer's contribution to pressure loss is negligible. However, this is not the case for filters used in high flows with high porosity (for example, fibrous textile or foam filters).

Additional pressure losses occur due to friction losses created by the flow along the square channels of the filter. This pressure loss, linearly dependent on the channel velocity for laminar flow, is expressed for a channel of length L as:

$$\Delta P_{friction} = \frac{\mu U L}{a^2} 2 c_f Re \xi \tag{23}$$

Here, $c_f Re$, constant for a square-profile channel with laminar flow, has a value of 14.227 and is shown as:

$$F = 2 c_f Re \tag{24}$$

Additionally, there are inertia losses due to contractions and expansions as the flow enters and exits the filter channels. This component increases in relation to the square of the axial entry velocity:

$$\Delta P_{contraction/expansion} = \zeta \frac{\rho U^2}{2} \tag{25}$$

where ζ is the contraction/expansion inertia loss coefficient dependent on the filter's flow cross-section and the Reynolds number.

Considering all these contributions, the total pressure loss of a clean filter is expressed as:

$$\Delta P = \frac{\mu Q}{2V_{filter}}(d_h + h_t)^2 \left[\frac{h_t}{\sigma_w d_h} + \frac{8FL^2}{3{d_h}^4}\right] + \frac{\rho Q^2 (d_h + h_t)^4}{{V_{filter}}^2 {d_h}^2}\left[\frac{\beta h_t}{4} + 2\zeta\left(\frac{L}{d_h}\right)^2\right] \tag{26}$$

Here, Q represents the flow rate, V_{filter} the effective filter volume, ζ the contraction/expansion ratio, and σ_w the wall permeability.

In conducted studies, a high level of repeatability has been observed in both flow and acoustic tests. The sensitivity of each measurement device used in the test setups is significantly higher than the level required by this study. Calibration has been applied before measurements to ensure the signals' accuracy from the microphones. Errors related to the sources specified below have been minimized with conducted studies in transmission loss and pressure loss curves.

The inlet diameter is 57 mm, and the distance between microphones is 30 mm and 60 mm. Considering the test conditions, the speed of sound is 343.2 m/s. Accordingly, the upper cutoff frequency is 3500 Hz according to Equations (18) and (19). The lower cutoff frequency has been determined as 50 Hz according to Equation (16).

Phase misalignment between microphones is one of the sources of error in acoustic measurements. This error source can be prevented by repeating measurements with the locations of the microphones changed. Although the impact of this error source has been seen to be minimal in conducted studies, phase misalignment has been corrected considering this factor.

Ambient noise plays a disruptive role in acoustic measurements. The presence of noise at a specific frequency in the environment reduces the accuracy of measurements at those frequencies. Noise isolation has been applied to the measurement environment to prevent this situation. Standards in this regard specify that the noise created by the sound source must be at least 10 dB higher in every frequency component than the ambient noise. This difference has been seen to be at least 20 dB in examinations.

The principle in determining the sound source is that the produced acoustic energy remains sufficient until the end of the test piece. Therefore, a sound source capable of providing a sound pressure level of 100 dB (Reference pressure: 20×10^{-6} Pa) has been used. Thus, the effect of ambient noise and flow noises has been prevented. Another source of error in transmission loss measurements arises in creating impedance boundary conditions. As described in the theoretical basis section, the measured pressure level must be different at every frequency to ensure the linear independence of equations. This has been examined in conducted studies, and it has

been seen that this condition is met with “open end” and “approximately anechoic termination” by adjusting the sensitivity of the sound source and microphones.

Back pressure measurements are conducted by modifying the flow and measuring the back pressure for each speed value. However, the pressure gauge and air source react differently to changes in the flow due to mechanical and electrical effects. This error source, known as hysteresis, has been mitigated by averaging the conducted measurements. Another error source is the additional transmission loss arising from the sound absorption and transmission of the channel in the test setup. This error can be eliminated by subtracting the transmission loss of the test tube from the filter’s transmission loss curve. In conducted studies, this value has been observed to be less than 0.5 dB for every frequency and it was decided that subtraction was unnecessary.

Flow and acoustic measurements were utilized to verify the accuracy of results obtained through mathematical models. Furthermore, test measurements enabled the examination of the impact of assumptions made in other methods on the results. Below, the transmission loss and pressure loss curves obtained from measurements on diesel particulate filters are presented.

To demonstrate the functionality of the established test setup and to gain insight for future measurements, measurements were conducted on four diesel particulate filters with different geometric characteristics. These four filters are different from the filters that will be used in the comparison.

The Transmission Loss (TL) curves obtained for the four diesel particulate filters (DPFs) under flow conditions are presented in **Figure 6**. These curves were generated using MATLAB’s measurement data and custom-built codes. Measurements were conducted at a flow speed corresponding to 0.4 Mach, which was chosen to simulate typical operating conditions. The TL curves exhibit notable variations across the different DPF designs, particularly in the mid-frequency range (1000–3000 Hz), where the interaction between flow dynamics and acoustic attenuation is most pronounced. This variation indicates that the geometry and porous properties of the DPF channels significantly impact their acoustic performance under flow. Additionally, the differences observed in TL values between the filters highlight the sensitivity of these measurements to changes in channel width, wall thickness, and porosity, which are key parameters in optimizing both noise reduction and emission control.

Figure 6 (**Figure 6a–d**) also illustrates the impact of flow-induced noise on the TL measurements, where fluctuations in transmission loss are more pronounced. The presence of flow creates additional complexities in the acoustic measurements due to turbulence and changes in the impedance boundary conditions, especially at higher frequencies. These fluctuations suggest that DPF designs with higher cell densities (e.g., DPF-3 and DPF-4) may be more susceptible to flow-induced noise, potentially reducing their effectiveness in real-world applications. However, it is essential to note that the repeatability of these measurements slightly decreases under flow conditions. This reduction in repeatability can be attributed to the noise created by the airflow and the inherent difficulties in maintaining stable impedance conditions during testing. Despite these challenges, the overall trends remain consistent across multiple test runs, confirming the validity of the test setup and measurement procedures. To mitigate the effects of flow-induced noise, subsequent analyses were conducted under no-flow conditions to establish baseline acoustic performance.

Pressure loss is another critical factor influencing DPF performance, which directly affects engine efficiency. **Figure 7** (**Figure 7a–d**) displays the pressure loss curves for the four DPFs tested, each having distinct geometrical characteristics. As seen in the figure, filters with larger diameters and thicker walls (e.g., DPF-3) tend to exhibit higher backpressure. High-pressure loss signifies a reduction in engine efficiency, as it increases the backpressure, leading to the re-entry of exhaust gases into the combustion chamber. This re-circulation reduces the volume of fresh air and fuel mixture entering the engine, decreasing overall engine performance. Therefore, minimizing pressure loss is a key objective in DPF design. The data obtained from these experiments were analyzed using MATLAB-generated codes, which helped estimate the magnitude of pressure loss under various flow conditions. These results were then used as part of a multi-objective optimization strategy to balance acoustic performance (TL) with pressure drop, ensuring that both noise attenuation and engine efficiency were maximized simultaneously.

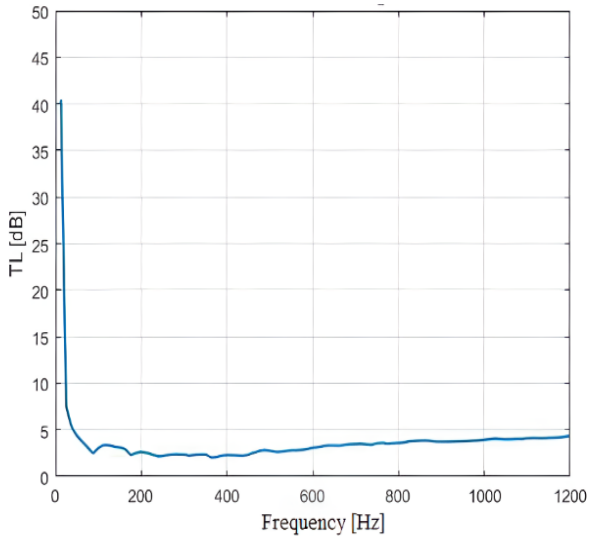

(**a**) DPF–1

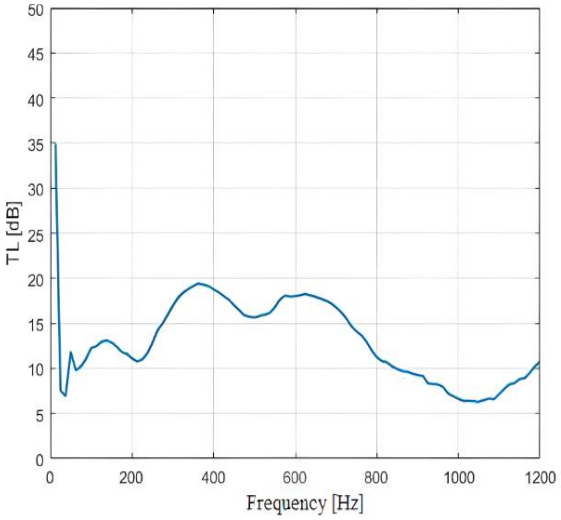

(**b**) DPF–2

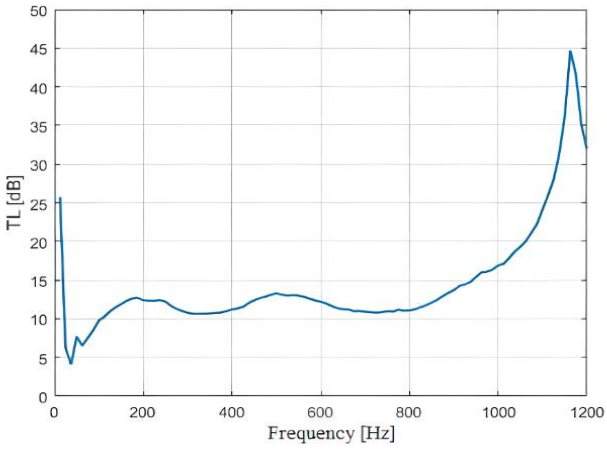

(**c**) DPF–3

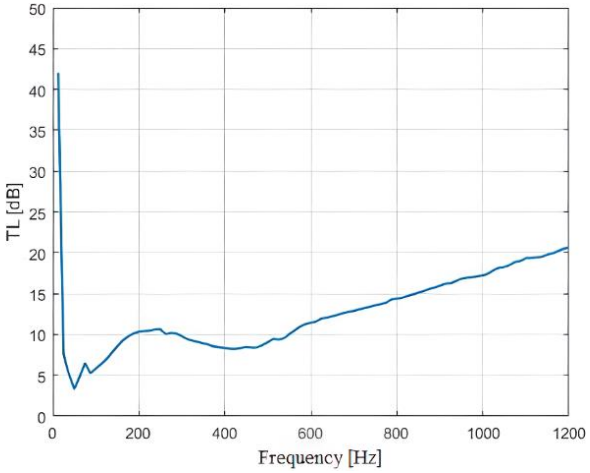

(**d**) DPF–4

Figure 6. STL curves.

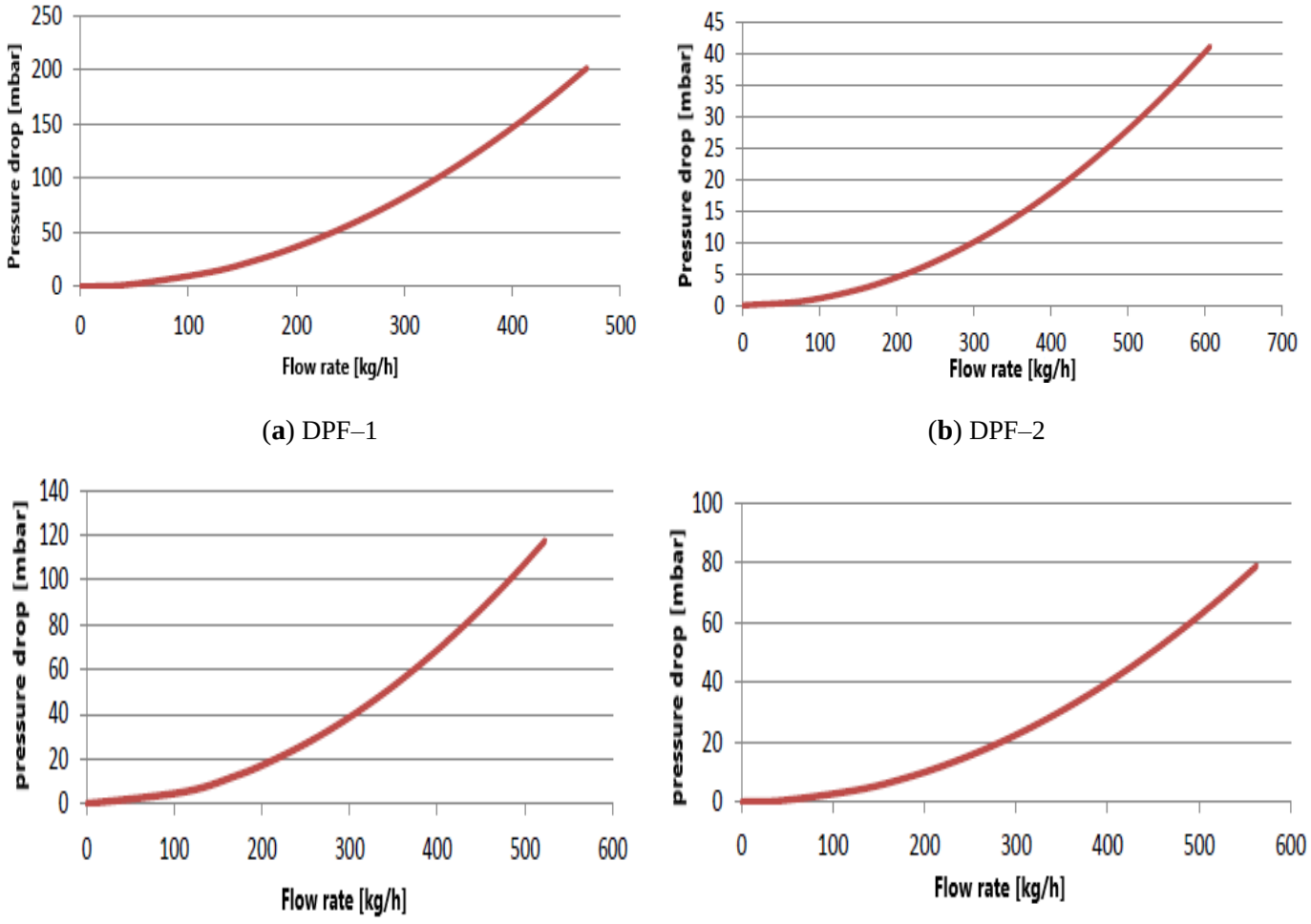

Figure 7. Pressure loss curves.

The technical specifications of the acquired diesel particulate filters are presented in **Table 1**.

Table 1. Dimensions of the DPFs used in the experiment.

	L152.4-90	**L152.4-150**	**L205-90**	**L203-150**
Cell density [CPSI]	90	150	90	150
Wall thickness [mm]	0.76	0.51	0.76	0.51
Wall width [mm]	2.50	1.70	2.50	1.70
Diameter [mm]	118	118	118	118
Length [mm]	152.40	152.40	205	203
Open area at the entrance [m^2]	0.25	0.28	0.25	0.28

Table 1 presents the technical specifications of the diesel particulate filters used in the study, highlighting key parameters such as cell density, wall thickness, and channel width. These dimensions directly influence the filters' TL and pressure loss performance. For instance, DPF-2 and DPF-4, with higher cell densities (150 CPSI), offer better acoustic attenuation but exhibit more significant pressure losses than DPF-

1 and DPF-3, which have lower cell densities (90 CPSI). The wall thickness also plays a critical role; thinner walls (0.51 mm) reduce pressure loss but can negatively affect noise reduction due to the reduced surface area for sound absorption. By understanding the interplay between these variables, it becomes clear that optimizing DPFs is a delicate balance between enhancing acoustic performance and maintaining efficient flow characteristics. The dimensions presented in **Table 1** serve as the basis for the multi-objective optimization conducted later in the study, where these parameters are fine-tuned to achieve the best possible outcomes in both TL and pressure loss.

Figure 8 shows four diesel particulate filters with different diameters and lengths. The STL curves were obtained using the test data and the mathematical model presented in **Figure 9** (**Figure 9a–d**).

Figure 8. Images of the DPFs used in the test.

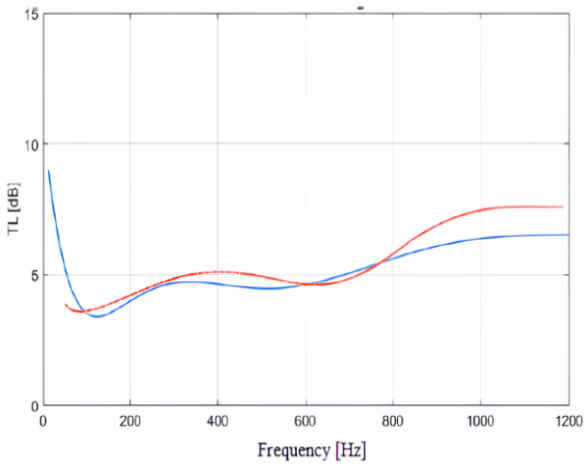

(**a**) L152.4–90 DPF

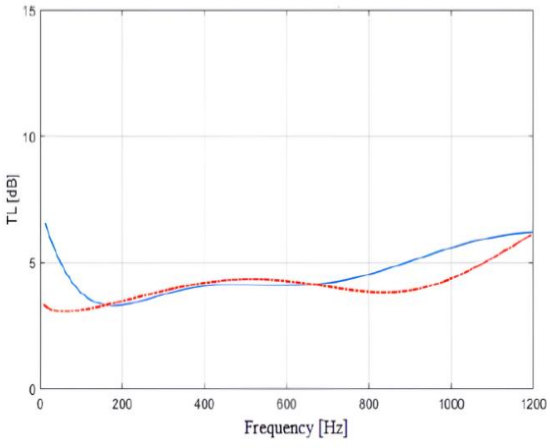

(**b**) L152.4–150 DPF

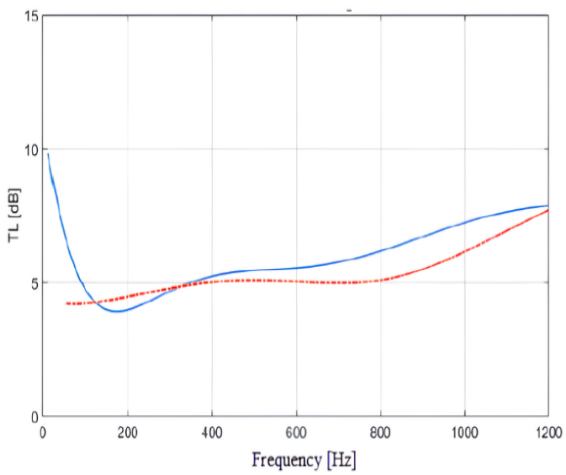

(**c**) L205–90 DPF

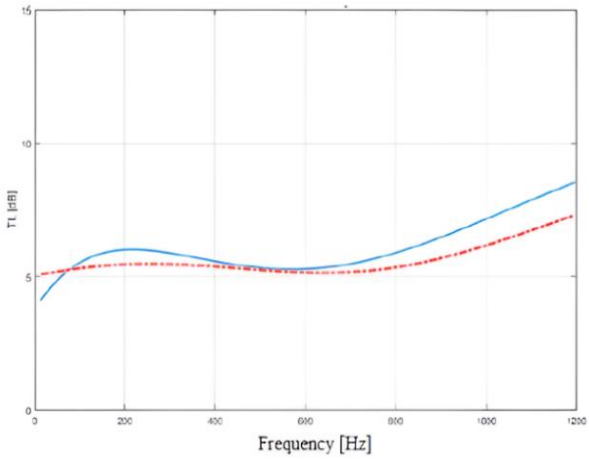

(**d**) L203–150 DPF

Figure 9. Test (blue) and mathematically modeled (red) STL curves.

Upon examining the figures obtained from test and analytical results, the STL curves are found to be entirely consistent. Differences arise from the manufacturer not providing clear information about specific properties, such as permeability material characteristics of the tested DPFs. These comparisons have led to the conclusion that the mathematical model validated by test studies is now usable for solving the optimization problem.

4. Effect of porous media properties on the acoustics of the DPF

A mathematical model was built to identify the acoustic behavior of the DPF according to the changes in the porous media properties. Among the porous media properties, the wall permeability, channel width, channel wall thickness and channel number were chosen for the analysis. The effects of each parameter were investigated individually. The pressure drop calculations were carried out for a constant flow rate. A DPF with 0.15 m diameter, a 0.25 m length, 0.00144 m channel width, 0.000355 m wall thickness, 2.5×10^{-13} m^2 wall permeability and 310,000 channels/m^2 was used as a reference for the calculations.

The pressure drop of a DPF was examined for different wall permeabilities, channel widths, channel wall thicknesses and channel numbers and listed in **Table 2**.

According to **Table 2**, the pressure drop decreases as the DPF wall permeability, the channel width and the channel number increases. However, the pressure drop increases as the DPF channel wall thickness increases.

First, the wall permeability effect on the acoustics was examined using five sets of DPF wall permeability values, 2.5×10^{-13} m^2, 3.0×10^{-13} m^2, 3.5×10^{-13} m^2, 4.0×10^{-13} m^2 and 4.5×10^{-13} m^2. The graph is shown in **Figure 10**.

Table 2. The pressure drop of a DPF for the porous media properties.

Pressure drop [mbar]												
σ [$\times 10^{-13}$ m^2]	**2.5**	107.99	d_h [$\times 10^{-3}$ m]	**0.8**	942.63	h_t [mm]	**0.3**	94.07	N [cpsi]	**90**	181.78
	3.0	99.62		**0.9**	577.70		**0.4**	120.24		**120**	135.49
	3.5	93.64		**1.0**	380.47		**0.5**	150.41		**150**	107.99
	4.0	89.16		**1.1**	265.74		**0.6**	184.85		**180**	89.77
	4.5	85.67		**1.2**	194.88		**0.7**	223.82		**210**	76.80

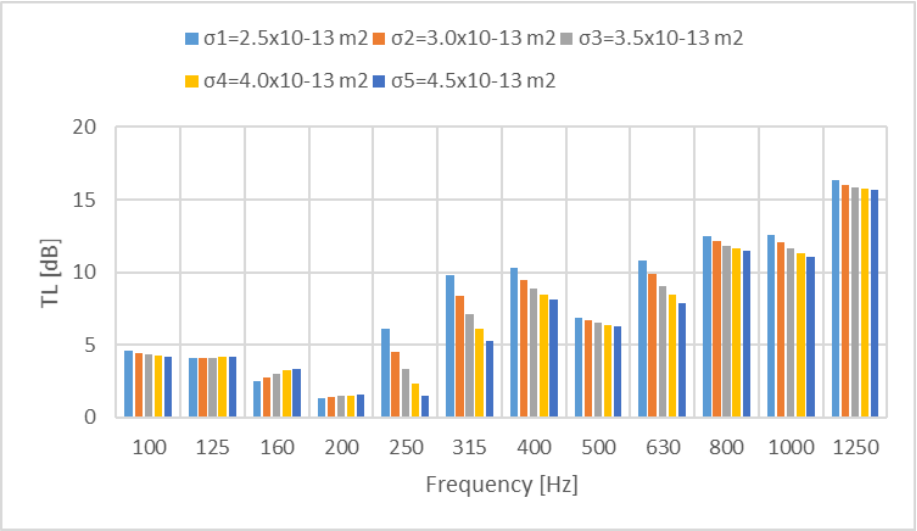

Figure 10. TL for five different DPF wall permeabilities.

As shown in **Figure 10**, as the wall permeability of the DPF increases, the TL decreases. An increase in wall permeability means a decrease in the wall surface area of channels that absorb sound, and this causes more noise to pass through the DPF.

To study the effect of the DPF channel width on the TL, calculations were carried out in the value range of 0.0008–0.0012 m, and the results are plotted in **Figure 11**.

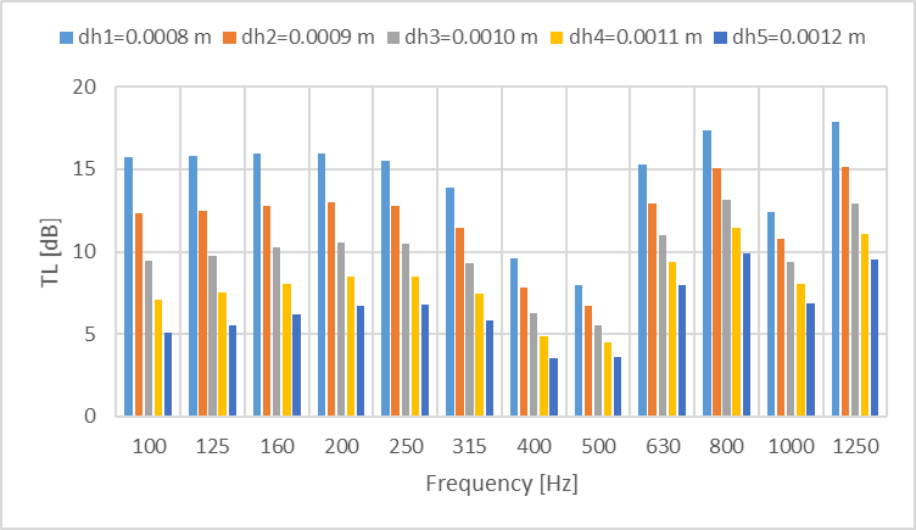

Figure 11. TL for five different DPF channel widths.

From the figure, it can be noted that when the DPF channel width increases, the TL decreases. An increase in the channel width means an increase in the space inside the DPF, which causes the channels to absorb less sound; hence, the TL decreases.

Another porous media property is the DPF channel wall thickness. DPF channel wall thicknesses of 0.0003 m, 0.0004 m, 0.0005 m, 0.0006 m and 0.0007 m were used to investigate its effect on the TL. **Figure 12** shows the results.

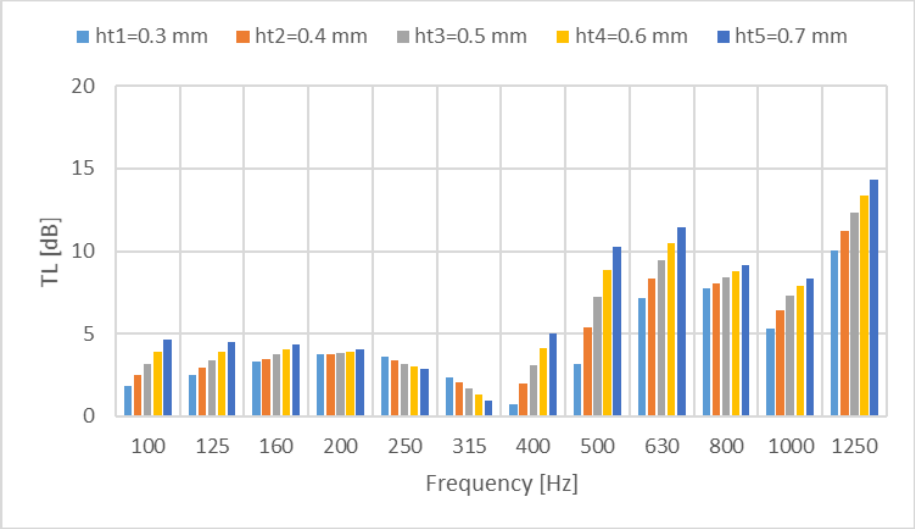

Figure 12. TL for five different DPF channel wall thicknesses.

By analyzing the TL curves in **Figure 12**, it can be said that the thicker the DPF channel wall is, the better TL values are obtained. As the DPF channel wall thickness increases, the surface-to-volume ratio inside the channels increases; hence, TL increases.

The TL calculations were performed for five different values of channel number, 90 cpsi, 120 cpsi, 150 cpsi, 180 cpsi and 210 cpsi, and the pressure drop was also calculated for the same channel number values. The results are shown in **Figure 13**.

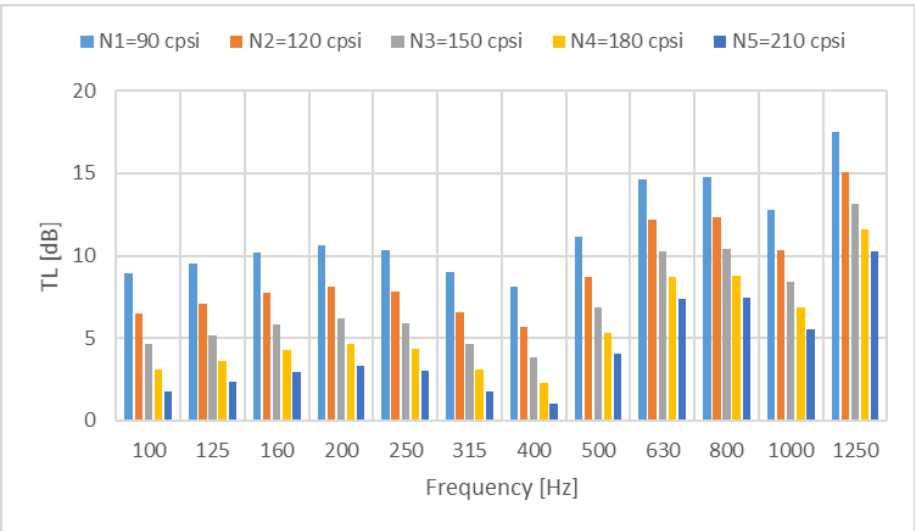

Figure 13. TL for five different DPF channel numbers.

It can be noted from **Figure 13** that the TL decreases as the number of channels increases. With the increase in the DPF channel number, the DPF takes on a cylindrical hole form, so the sound absorption and, thereby, the TL decrease. The increase in the DPF channel number also means an increase in the DPF wall permeability. As mentioned before, an increase in the DPF wall permeability causes a decrease in the TL.

5. Optimization of the DPF

This study performs a multi-objective optimization to optimize the acoustics and the pressure drop of the DPF based on the porous media properties. The acoustic part of the optimization involves maximizing the sum of the values of the TL parameter at all frequencies, which is calculated as follows:

$$TL_{total} = 10 \times \left(\sum_{i} 10^{TL_i/10} \right) \tag{27}$$

In the pressure drop part of the optimization, we aimed to minimize the pressure drop for a more efficient engine operation. The optimization problem was performed using the NSGA-II algorithm, and the code was written in MATLAB. This study chose four porous media properties, the DPF channel width, wall permeability, channel number and channel wall thickness, as design variables for the optimization problem. When specifying the boundaries for the design variables, it is considered that the DPF can be manufactured. Optimization was carried out several times for different iteration numbers, populations, and generation sizes to avoid local extremum points. Finally, population sizes of 200 and 500 generations were used in the algorithm, and the obtained Pareto Front is illustrated in **Figure 14**. A Pareto Front can show the results of the searches for the best value for one of the objective functions by requiring that the other does not worsen. Objectives 1 and 2 represent maximizing the TL and minimizing the pressure drop, respectively, converging to the region in the red circle. The proposed results within that circle were examined closely to determine if the DPF having these optimum parameter values is producible or not and if there are misleading results caused by single TL maxima that may affect the total TL.

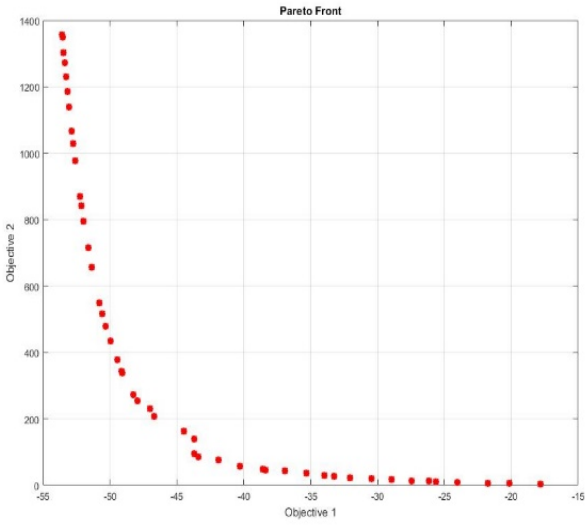

Figure 14. Pareto Front for two objective functions.

Some of the solutions obtained using NSGA-II for two objective functions are shown in **Table 3**.

Table 3. Optimum parameter values for the solution obtained using NSGA-II.

TL_{OA} [dB]	Pressure drop [mbar]	d_h [m]	σ_w [m^2]	N [cpsi]	h_t [m]
9.33	14.50	0.002363	4.85×10^{-13}	90	0.000100
9.93	16.21	0.002279	4.83×10^{-13}	90	0.000100
22.40	327.36	0.001408	5.00×10^{-13}	90	0.000800
21.22	195.22	0.001160	4.85×10^{-13}	90	0.000121
26.67	1007.63	0.001218	1.50×10^{-13}	90	0.000800
21.73	268.79	0.001495	5.00×10^{-13}	90	0.000800

After examining the results individually, the optimum parameter values were chosen from **Table 2** and listed in **Table 4**.

Table 4. Optimum parameter values obtained using NSGA-II.

Parameter	Optimum Parameter Value
DPF wall permeability, σ_w [m^2]	5×10^{-13}
DPF channel width, d_h [m]	0.001495
DPF channel wall thickness, h_t [m]	0.0008
DPF channel number, N [cpsi]	90

The optimum DPF parameter values that supply the best TL and pressure drop values in the range of interest obtained using NSGA-II were used to calculate the TL graph. The graph is shown in **Figure 15**.

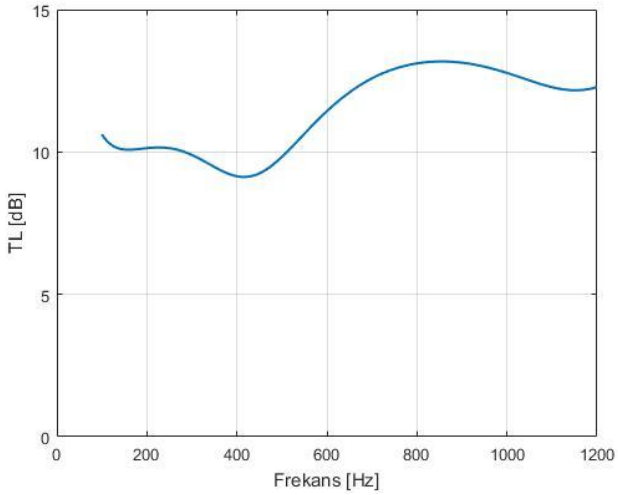

Figure 15. TL for the optimum DPF.

6. Conclusions

First, a mathematical model was built to determine the TL and the pressure drop for a DPF. TL calculations were carried out using the transfer matrix method in the literature, and the results were given in the 0–1200 Hz frequency range.

A mathematical model was constructed to examine the effects of the individual porous media properties on acoustics. As a result of these parametric studies, it was determined that the transmission losses are proportional to the channel wall thickness but not to the wall permeability, channel number or channel width. The pressure drop property was also investigated and it was determined that the pressure drop is proportional to the channel wall thickness but not to the wall permeability, channel number or channel width.

After studying the effects of the individual porous media properties on the acoustics and the pressure drop property, a multi-objective optimization was carried out using the NGSA-II algorithm. The optimization problem was built to provide the maximum TL and the minimum pressure drop for the DPF according to porous media properties. Many iterations were performed to prevent being stuck in a local extremum point. As a result, the DPF wall permeability, channel width, channel wall thickness and the channel number for the optimum DPF were defined as 5×10^{-13} m^2, 0.001495 m, 0.0008 m and 90 cpsi (channels per square inch), respectively.

Author Contributions: Sinem Ozturk was responsible for the conceptualization of the study, experimental setup design, and data collection. Sinem Ozturk also conducted the multi-objective optimization and analyzed the results. Haluk Erol supervised the research, provided critical feedback on the experimental design, and contributed to refining the research methodology. Both authors collaborated in interpreting the data and writing the manuscript. Sinem Ozturk took the lead in drafting the manuscript, while Haluk Erol contributed significantly to revising and editing the content. Both authors approved the final version of the manuscript for submission.

Author contributions: Conceptualization, SO and HE; formal analysis, SO and HE; data curation, SO and HE. All authors have read and agreed to the published version of the manuscript

Availability of data and materials: The experimental data used to support the finding of the present study is available from the corresponding author upon request.

Conflict of interest: The authors declare no conflict of interest.

References

1. G. Konstandopoulos, J. H. Johnson, “Wall-flow diesel particulate filters - their pressure drop and collection efficiency”, Society of Automotive Engineering, SAE Paper No. 890405, 1989.
2. S. Allam, M. Abom, “Acoustic modeling and testing of diesel particulate filters”, Journal of Sound and Vibration, 288, 255-273, 2005.
3. E. Dokumaci, “Sound transmission in pipes with porous walls”, Journal of Sound and Vibration, 329, 5346-5355, 2010.
4. G. Wenzhi, F. Liming, “FEM analysis on acoustic performance of wall-flow diesel particulate filters", Chinese Journal of Mechanical Engineering, 24, 2011.

5. S.M. Fayyad, M.N. Hamdan, S. Abu-Ein, "Four-port noise model for the diesel particulate filters (DPF)", Jordan Journal of Mechanical and Industrial Engineering, 5, 495-507, 2011.
6. Z.G. Liu, R.K. Miller, "Flow distributions and pressure drops of wall-flow diesel particulate filters", Society of Automotive Engineering, SAE Paper, 2002, 2002011311.
7. Katari, M. Syed, M. Sickels, T. Wahl, S. Rajadurai, "Effect of aspect ratio on pressure drop and acoustics in diesel particulate filters", SAE International, 2004, 2004010695.
8. Zhang, Z., Dong, R., Lan, G., Yuan, T., & Tan, D. (2023). Diesel particulate filter regeneration mechanism of modern automobile engines and methods of reducing PM emissions: A review. Environmental Science and Pollution Research. Springer.
9. Tan, P., Wang, D., Yao, C., Zhu, L., Wang, Y., Wang, M., & Hu, Z. (2020). Extended filtration model for diesel particulate filter based on diesel particulate matter morphology characteristics. Fuel, Elsevier.
10. Lisi, L., Landi, G., & Di Sarli, V. (2020). The issue of soot-catalyst contact in regeneration of catalytic diesel particulate filters: A critical review. Catalysts, MDPI.
11. Zhang, Z., Dong, R., Tan, D., Duan, L., Jiang, F., & Yao, X. (2023). Effect of structural parameters on diesel particulate filter trapping performance of heavy-duty diesel engines based on grey correlation analysis. Energy, Elsevier.
12. Meng, Z., Wang, W., Zeng, B., Bao, Z., Hu, Y., & Ou, J. (2023). An experimental investigation of particulate emission characteristics of catalytic diesel particulate filters during passive regeneration. Chemical Engineering Science, Elsevier.
13. F. Payri, A. Broatch, J.R. Serrano, P. Piqueras, “Experimental-theoretical methodology for determination of inertial pressure drop distribution and pore structure properties in wall-flow diesel particulate filters (DPF)”, Energy, 36, 6731-6744, 2011.
14. S. M. Fayyad, “Reducing noise and emissions of automobiles using diesel particulate filters”, Proceedings of the 14th International Conference on Environmental Science and Technology, Rhodes, Greece, 3-5 September, 2015.
15. W. Momani, “Effect of porous media properties on transmission losses of a diesel particulate filter unit”, Journal of Engineering Sciences, 36-4, 813- 824, 2008.
16. C. E. Sprouse III, M.D. Mangus, C.D. Depcik, “Diesel particulate filter model with detailed permeability analysis”, Proceedings of the ASME 2011 International Mechanical Engineering Congress & Exposition IMECE 2011, Denver, Colorado, USA, 11-17 November, 2011.
17. G. A. Stratakis, D. L. Psarianos, A. M. Stamatelos, “Experimental investigation of the pressure drop in porous ceramic diesel particulate filters”, Journal of Automobile Engineering, 216, 773- 784, 2002.
18. M. Masoudi, A. Heibel, P.M. Then, “Predicting pressure drop of Wall-flow diesel particulate filters-theory and experiment”, Society of Automotive Engineering, SAE Paper, 2000; 2000010184.
19. J. Michelin, B. Figueras, C. Bouly, B. France, D. Maret, “Optimized Diesel Particulate Filter System for Diesel Exhaust Aftertreatment,” Society of Automotive Engineering, SAE Paper, Vol. 2000, no. 724, 2000.
20. C. Barataud, S. Bardon, B. Bouteiller, and V. Gleize, “Diesel Particulate Filter Optimization Reprinted From: Diesel Exhaust Emissions Control,” Society of Automotive Engineering, SAE Paper, No. 724, 2003.
21. S. Ozturk and H. Erol, “Multi-objective optimization of a diesel particulate filter: an acoustic approach,” Part. Sci. Technol., vol. 40, no. 4, pp. 465–474, 2022.
22. F. Jun, G. Jinke, L. Yunqing, J. Guohai, “Study on Structure Optimization of Diesel Particulate Filter Based on Flow Field Distribution Characteristics,” 2011 Int. Conf. Comput. Distrib. Control Intell. Environ. Monit., no. 1, pp. 616–619, 2011.
23. S. Fujii, T. Asako, K. Yuuki, “Studies of diesel particulate filter performances by a diesel engine simulator”, SAE International, 2010; 2010010813.
24. J. T. Hicks, W. E. Hill, A.J. Kotrba, “DPF acoustic performance: an evaluation of various substrate materials and soot conditions”, SAE International, 2011; 2011012198.
25. J. H. Johnson, A. G. Konstandopoulos, “A study describing the performance of diesel particulate filters during loading and regeneration- a lumped parameter model for control applications”, SAE Journal, 2003; 2003010842.
26. D. E. Goldberg, Genetic Algorithms in Search Optimization and Machine Learning. USA: Addison Wesley Publishing Company, 1989
27. Konstandopoulos, A.G. (2003). Flow Resistance Descriptors for Diesel Particulate Filters: Definitions, Measurements and Testing, SAE Tech. Pap. Ser., 2003–01–08, no. 724.